GEOPHYSICS, VOL. 87, NO. 6 (NOVEMBER-DECEMBER 2022); P. M247–M258, 13 FIGS.
10.1190/GEO2021-0747.1





# Petrophysical inversion based on *f-s-r* amplitude-variation-with-offset linearization and canonical correlation analysis

Dario Grana[1], Brian Russell[2], and Tapan Mukerji[3]

## ABSTRACT

The prediction of petrophysical properties, such as porosity and rock-fluid volumes, from partially stacked seismic data typically requires a rock-physics model that often is lithology dependent and difficult to calibrate. We adopt canonical correlation analysis (CCA) to infer the underlying relation between petrophysical properties and elastic attributes estimated from seismic data. We develop a two-step inversion approach: first, we predict elastic properties from partially stacked seismic data using a Bayesian linear inverse method based on an amplitude-variation-with-offset (AVO) linearization in terms of fluid, rigidity, and density factors, and then we predict petrophysical properties from the estimated AVO attributes using CCA. The novelty of our approach is the application of CCA to the fluid and rigidity factors, which avoids the calibration of an explicit rock-physics model by automatically deriving a linear relation in the lower dimensional space of the canonical variables. The parameterization of the linearization in terms of fluid, rigidity, and density factors maximizes the correlation with respect to the petrophysical properties of interest. Furthermore, the probabilistic approach is extended to the petrophysical inversion using Bayesian linear theory and the posterior distribution of petrophysical properties conditioned by seismic data is computed by combining the probability distributions obtained from seismic and petrophysical inversion to propagate the uncertainty from the seismic to the petrophysical domain. The inversion is validated on a synthetic case that finds high accuracy of our formulation. A case study with synthetic and real partially stacked seismic data also is presented and compared to a traditional inversion with an explicit rock-physics model.

## INTRODUCTION

The prediction of petrophysical properties from seismic data requires a rock-physics model to relate the petrophysical properties to their elastic response and a seismic forward model to link elastic properties to their seismic response (Grana et al., 2021). In seismic reservoir characterization studies, the seismic forward operator often is approximated with amplitude-variation-with-offset (AVO) models (Avseth et al., 2010), whereas the rock-physics model depends on the geologic environment and is empirically calibrated using well-log data and core samples (Mavko et al., 2020).

Seismic AVO methods are commonly used in reservoir characterization to predict elastic attributes from partially stacked seismic data. These attributes represent physical properties related to stiffness, density, and wave velocities, and they are interpreted in terms of rock and fluid properties. AVO formulations are generally expressed as a combination of three terms associated with three elastic attributes, with the coefficients of the combination depending on the incidence angle. Several AVO parameterizations have been presented, including P- and S-wave velocities, density, P- and S-impedances, elastic moduli, and nonlinear combinations of these parameters (Bortfeld, 1961; Richards and Frasier, 1976; Aki and Richards, 2002).

AVO formulations provide a mathematically tractable approximation to the equations for the calculation of the amplitudes of the reflected and transmitted waves as derived by Knott (1899) and Zoeppritz (1919). The most common AVO approximation is the Aki-Richards' equation (Aki and Richards, 2002), where the P-wave

Manuscript received by the Editor 29 November 2021; revised manuscript received 24 June 2022; published ahead of production 14 July 2022; published online 8 September 2022.
[1]University of Wyoming, Department of Geology and Geophysics, Laramie, Wyoming, USA. E-mail: dgrana@uwyo.edu (corresponding author).
[2]GeoSoftware, Calgary, Alberta, Canada. E-mail: brian.russell@cgg.com.
[3]Stanford University, Department of Energy Resources Engineering, Stanford, California, USA. E-mail: mukerji@stanford.edu.

reflectivity coefficients are approximated as a linear combination of the reflectivity terms associated with P- and S-wave velocities and density. This linear formulation can be used in seismic inversion to calculate the unknown values of P- and S-wave velocities and density from the seismic amplitudes using least-square methods. Alternatively, this formulation can be used to derive a Bayesian linearized method for seismic inversion and predict the posterior distribution of P- and S-wave velocities and density, as proposed in Buland and Omre (2003).

Gidlow et al. (1992) and Fatti et al. (1994) propose a different parameterization expressed in terms of P- and S-impedance and density, by rearranging Aki-Richards' formulation. Shuey (1985) replaces the shear-velocity term with the Poisson ratio. Gray et al. (1999) propose two parameterizations: the *l-m-r* formulation expressed in terms of the Lamé modulus $\lambda$, the shear modulus $\mu$, and the density $\rho$, and the *k-m-r* formulation expressed in terms of the bulk modulus $K$, the shear modulus $\mu$, and the density $\rho$. This parameterization is based on the AVO formulation proposed by Goodway et al. (1997) based on the Lamé elastic parameters. Russell et al. (2003) generalize the approaches presented in Goodway et al. (1997) and Gray et al. (1999) by combining them with the poroelastic relations proposed by Biot (1941) and Gassmann (1951). According to the Russell et al. (2003) general formulation, the weights of the AVO approximation depend on the incidence angle and two elastic constants, specifically the $V_P/V_S$ ratio in saturated conditions and the $V_P/V_S$ ratio in dry conditions. Russell et al. (2011) propose a new AVO linearized formulation expressed in terms of the fluid-porosity factor $f$ (henceforth called the fluid factor for simplicity), the shear modulus $\mu$, and the density $\rho$. The approaches presented in Goodway et al. (1997) and Gray et al. (1999) then become specific cases of the formulation in Russell et al. (2011). In this work, we adopt a formulation based on Russell et al. (2011), where we replace the shear modulus $\mu$ with the rigidity factor $s$ (also referred to as solid factor). We refer to this formulation as the *f-s-r* formulation, and we correlate these variables to the petrophysical properties of interest.

The available AVO formulations provide a powerful tool for quantitative seismic interpretation; however, the current parameterizations do not provide intuitive parameters for the evaluation of porosity nor rock and fluid volumetric fractions. It is known that high velocity is generally associated with low porosity and that a high $V_P/V_S$ ratio might be an indicator of shale presence; however, the quantification of porosity, mineral volumes, and fluid saturations requires rock-physics models that link the petrophysical properties to the elastic properties, such as those proposed by Avseth et al. (2010), Dvorkin et al. (2014), and Mavko et al. (2020). Seismic AVO inversion for elastic properties (Goodway et al., 1997; Connolly, 1999; Whitcombe et al., 2002; Buland and Omre, 2003; Hampson et al., 2005) can be integrated with rock-physics models in a process that is referred to as petrophysical inversion, and also can be performed with probabilistic methods (Bosch, 1999; Mukerji et al., 2001; Mazzotti and Zamboni, 2003; Bornard et al., 2005; Coléou et al., 2005; Bachrach, 2006; Gunning and Glinsky, 2007; Buland et al., 2008; González et al., 2008; Spikes et al., 2008; Bosch et al., 2009; Avseth et al., 2010; Grana and Della Rossa, 2010; Rimstad et al., 2012; Connolly and Hughes, 2016; Grana, 2016; Aleardi and Ciabarri, 2017; Grana et al., 2017; Aleardi et al., 2018a, 2018b; Fjeldstad and Grana, 2018).

Rock-physics models must be calibrated using core samples or well-log data, as they often include empirical parameters. The calibration and the integration of the rock-physics relations in the AVO formulation are generally challenging due to the spatial variations of the rock-physics model parameters and the nonlinearity of the model. For this reason, we propose to define an implicit relation between AVO attributes and petrophysical properties using canonical correlation analysis (CCA). CCA finds linear combinations between two sets of variables that maximize their pair-wise linear correlations (Thompson, 1984; Hardoon et al., 2004). CCA has been applied in geoscience studies for facies classification (Fournier and Derain, 1995; Purkait and Majumdar, 2014), seismic reservoir characterization (Alvarez et al., 2015), interpretation of time-lapse seismic attributes (Wu et al., 2005), reservoir modeling forecasting (Satija et al., 2017), and geologic modeling uncertainty quantification (Yin et al., 2020). However, CCA has not been used in the context of petrophysical inversion.

We propose a petrophysical inversion consisting of two steps: (1) Bayesian linearized inversion of partially stacked seismic data based on the *f-s-r* formulation (Russell et al., 2011) with respect to fluid and rigidity factors and density and (2) CCA to predict petrophysical properties from AVO attributes. The CCA-based petrophysical inversion is formulated in the deterministic and Bayesian frameworks. The proposed application focuses on a clastic reservoir in which the properties of interest are porosity, clay volume, and water saturation, but the method can be applied to any geologic environment with any finite set of petrophysical variables.

## METHOD

### Theoretical background

In AVO studies, the seismic response of a sequence of fluid-saturated porous rocks can be computed using a seismic convolutional model (Russell, 1988; Aki and Richards, 2002), in which the seismic amplitudes are approximated by convolution of a known source wavelet $w$ and the vector of reflection coefficients $r_{PP}$. The reflection coefficients represent the angle-dependent reflectivity magnitudes of the elastic contrasts at the interfaces. For an incidence angle $\theta$, the seismic signal $d(t,\theta)$ can be expressed as a function of the two-way traveltime $t$ as

$$d(t,\theta) = w(t,\theta) * r_{PP}(t,\theta) = \int w(t,\theta) r_{PP}(t-u,\theta) du, \quad (1)$$

where $*$ is the convolution operator. However, for weak elastic contrasts and small incidence angles, linear approximations are commonly used (Aki and Richards, 2002). The Aki-Richards' approximation (Aki and Richards, 2002) is the most common linearization of Zoeppritz equations, where the reflectivity coefficients $r_{PP}(t,\theta)$ are approximated as a function of P- and S-wave velocity, $V_P(t)$ and $V_S(t)$, and density $\rho(t)$. Aki-Richards' equation can be written as a time-continuous reflectivity function (Stolt and Weglein, 1985) as follows:

$$r_{PP}(t,\theta) = c_P(\theta)\frac{\partial}{\partial t}\ln V_P(t) + c_S(\theta)\frac{\partial}{\partial t}\ln V_S(t) + c_\rho(\theta)\frac{\partial}{\partial t}\ln \rho(t), \quad (2)$$

with angle-dependent coefficients given by

$$\begin{cases} c_P(\theta) = \frac{1}{2}(1+\tan^2\theta) \\ c_S(\theta) = -\frac{4}{\gamma^2}\sin^2\theta \\ c_\rho(\theta) = \frac{1}{2}(1-\frac{4}{\gamma^2}\sin^2\theta) \end{cases}, \quad (3)$$

where $\gamma = \overline{V_P}/\overline{V_S}$ is the ratio of the average $\overline{V_P}$ and $\overline{V_S}$ of fluid-saturated porous rocks.

Among the several reparameterizations of equation 2, Russell et al. (2011) propose a linear formulation that involves a fluid term $f$, a rigidity factor $s$, and density $\rho$, based on the Krief et al. (1990) synthesis of the poroelasticity theory of Biot (1941) and Gassmann (1951). The fluid and rigidity factors are defined according to poroelasticity theory (Russell et al., 2011) as

$$f = \frac{\left(1-\frac{K_{dry}}{K_{sol}}\right)^2}{\frac{\phi}{K_{fl}} + \frac{(1-\phi)}{K_{sol}} - \frac{K_{dry}}{K_{sol}^2}}, \quad (4)$$

$$s = K_{dry} + \frac{4}{3}\mu_{dry}, \quad (5)$$

where $K_{dry}$ is the dry-rock bulk modulus, $K_{sol}$ is the solid-phase bulk modulus, $K_{fl}$ is the fluid-phase bulk modulus, $\phi$ is porosity, and $\mu_{dry} = \mu_{sat}$ is the shear modulus of the porous rock. The fluid term is part of the Gassmann equation as $K_{sat} = K_{dry} + f$, whereas the rigidity factor represents the dry-rock compressional modulus $s = M_{dry}$. The fluid term $f$ is more completely written as $\alpha^2 M$, where $\alpha = (1-(K_{dry}/K_{sol}))^2$ is the Biot coefficient and $M = ((\phi/K_{fl}) + ((1-\phi)/K_{sol}) - (K_{dry}/K_{sol}^2))^{-1}$ is the Biot fluid modulus (Russell et al., 2011). Thus, although the $s$ term isolates the dry rock component, the $f$ term does not fully isolate the fluid component and contains a term involving the solid and dry-rock bulk moduli. However, the $f$ term is a sensitive indicator of changes in fluid content, more so than the commonly used $l$-$m$-$r$ approach (Goodway et al., 1997) as shown in Russell et al. (2011).

The $f$-$s$-$r$ AVO linearization can be then formulated as

$$r_{PP}(t,\theta) = c_f(\theta)\frac{\partial}{\partial t}\ln f(t) + c_s(\theta)\frac{\partial}{\partial t}\ln s(t) + c_r(\theta)\frac{\partial}{\partial t}\ln \rho(t), \quad (6)$$

with angle-dependent coefficients given by

$$\begin{cases} c_f(\theta) = \left(1-\frac{\gamma_{dry}^2}{\gamma^2}\right)\frac{\sec^2\theta}{4} \\ c_s(\theta) = \frac{1}{\gamma^2}\left(\frac{\sec^2\theta}{4} - \frac{2}{\gamma_{dry}^2}\sin^2\theta\right) \\ c_r(\theta) = \frac{1}{2} - \frac{\sec^2\theta}{4} \end{cases}, \quad (7)$$

where $\gamma_{dry} = (\overline{V_P}/\overline{V_S})_{dry} = (K_{dry}/\mu_{dry}) + (4/3)$. If the ratios $\gamma_{dry}$ and $\gamma$ are taken to be constant along the profile, then the reflection coefficients depend only on the angle $\theta$. The original formulation in Russell et al. (2011) is expressed in terms of $f, \mu_{dry} = s/\gamma_{dry}^2$, and $\rho$; however, in this work, we reformulate the linearization in terms of $f$, $s$, and $\rho$ to maximize the correlation between the rigidity factor and the mineral volume.

The fluid and rigidity factors can be computed from P- and S-wave velocities and density as

$$f = (\rho V_P)^2 - \gamma_{dry}^2(\rho V_S)^2, \quad (8)$$

$$s = \gamma_{dry}^2(\rho V_S)^2, \quad (9)$$

as shown in Russell et al. (2011). The fluid and rigidity factors and density are strictly related to petrophysical properties, such as porosity, mineral volumes, sorting, diagenesis, cementation, and fluid saturations. Figure 1 shows the correlations between the elastic attributes and the petrophysical properties: the linear correlations between fluid factor and saturation ($c(f, s_w) = 0.91$) and between porosity and density ($c(\rho, \phi) = -0.92$) are high, whereas the correlation between the rigidity factor and the clay volume

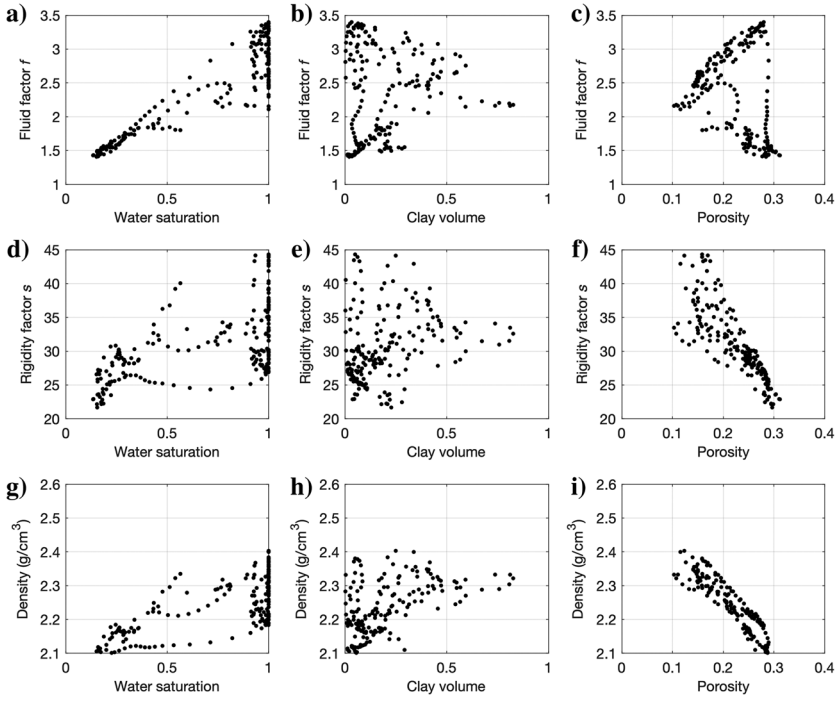


Figure 1. Correlations between $f$-$s$-$r$ elastic attributes and petrophysical properties: (a) fluid factor versus water saturation, (b) fluid factor versus clay volume, (c) fluid factor versus porosity, (d) rigidity factor versus water saturation, (e) rigidity factor versus clay volume, (f) rigidity factor versus porosity, (g) density versus water saturation, (h) density versus clay volume, and (i) density versus porosity.

$(c(s, v_c) = 0.23)$ is relatively low, due to the porosity effect on the shear modulus. Porosity affects all three elastic properties as the porosity is part of the fluid term, rigidity term, and density. Similarly, density is affected by all petrophysical properties as the density of the fluid-saturated porous rocks depends on fluid saturations, mineral fractions, and pore volume. The interdependence between petrophysical and elastic properties is one of the main sources of uncertainty as often observed in rock-physics modeling (Avseth et al., 2010).

Based on the correlation between the variables in the *f-s-r* AVO linearization and the petrophysical properties, we propose an innovative inversion method to predict petrophysical properties from seismic data. First, we predict the elastic attributes of the *f-s-r* formulation from partially stacked seismic data using a Bayesian linearized inversion, and then we estimate the petrophysical properties using CCA.

## Bayesian linearized *f-s-r* inversion

We first present a Bayesian linearized inversion *f-s-r* approach for the prediction of elastic attributes $\mathbf{m} = [f, s, \rho]$ from $n_\theta$ seismic angle stacks $\mathbf{d} = [d(\theta_1), \ldots, d(\theta_{n_\theta})]$, following the Bayesian linearized AVO inversion approach presented by Buland and Omre (2003). The forward model in the inversion is the convolution (equation 1) of a known source wavelet $w$ and the vector of reflection coefficients $r_{\mathrm{PP}}$ computed according to the *f-s-r* formulation (equation 6). The operator is linear in the logarithms of the fluid factor, rigidity factor, and density. The unknown model variables are represented by the vector $\mathbf{m} = [\ln \mathbf{f}, \ln \mathbf{s}, \ln \boldsymbol{\rho}]^T$ of length $n_m = 3(n_t + 1)$, where $n_t$ is the number of seismic measurements (corresponding to $n_t$ interfaces of $n_t + 1$ layers with unknown elastic properties).

The discretization of the continuous reflectivity series represented by the vector $\mathbf{c}$ of length $n_\theta n_t$ is given by

$$\mathbf{c} = \mathbf{A}\mathbf{D}\mathbf{m}, \tag{10}$$

where $\mathbf{A}$ is a matrix containing the discrete time samples of the coefficients $c_f(\theta), c_s(\theta)$, and $c_r(\theta)$ (equation 7) and $\mathbf{D}$ is a first-order differential matrix (Buland and Omre, 2003).

The seismic signal is represented by the vector $\mathbf{d}$ of length $n_\theta n_t$ and is computed as a discrete convolution (i.e., matrix-vector multiplication) of the wavelet matrix and the reflection coefficient vector $\mathbf{c}$:

$$\mathbf{d} = \mathbf{W}\mathbf{c} + \boldsymbol{\varepsilon} = \mathbf{W}\mathbf{A}\mathbf{D}\mathbf{m} + \boldsymbol{\varepsilon}, \tag{11}$$

where $\mathbf{W}$ is a block-diagonal matrix containing the discretized wavelets, one per angle, and $\boldsymbol{\varepsilon}$ is a vector of length $n_\theta n_t$ that represents the data errors. In equation 11, $\mathbf{W}$ is a band matrix of dimensions $(n_\theta n_t \times n_\theta n_t)$, $\mathbf{A}$ is a sparse block matrix of dimensions $(n_\theta n_t \times 3n_t)$, and $\mathbf{D}$ is a sparse block matrix of dimensions $(3n_t \times n_m)$. The structure of these matrices is the same as in Buland and Omre (2003) and Grana et al. (2021) and it is given in Appendix A.

We can rewrite equation 11 component by component as

$$\begin{bmatrix} d(t_1,\theta_1) \\ \vdots \\ d(t_{n_t},\theta_1) \\ d(t_1,\theta_2) \\ \vdots \\ \vdots \\ d(t_{n_t},\theta_{n_\theta}) \end{bmatrix} = \mathbf{W} \begin{bmatrix} c(t_1,\theta_1) \\ \vdots \\ c(t_{n_t},\theta_1) \\ c(t_1,\theta_2) \\ \vdots \\ \vdots \\ c(t_{n_t},\theta_{n_\theta}) \end{bmatrix} + \begin{bmatrix} \varepsilon(t_1,\theta_1) \\ \vdots \\ \varepsilon(t_{n_t},\theta_1) \\ \varepsilon(t_1,\theta_2) \\ \vdots \\ \vdots \\ \varepsilon(t_{n_t},\theta_{n_\theta}) \end{bmatrix}$$

$$= \mathbf{W}\mathbf{A}\mathbf{D} \begin{bmatrix} f(\tau_1) \\ \vdots \\ f(\tau_{n_t+1}) \\ s(\tau_1) \\ \vdots \\ s(\tau_{n_t+1}) \\ \rho(\tau_1) \\ \vdots \\ \rho(\tau_{n_t+1}) \end{bmatrix} + \begin{bmatrix} \varepsilon(t_1,\theta_1) \\ \vdots \\ \varepsilon(t_{n_t},\theta_1) \\ \varepsilon(t_1,\theta_2) \\ \vdots \\ \vdots \\ \varepsilon(t_{n_t},\theta_{n_\theta}) \end{bmatrix}, \tag{12}$$

where $t_1, \ldots, t_{n_t}$ are the time samples of the measurements (at the interfaces) and $\tau_1, \ldots, \tau_{n_t+1}$ are the time samples of the unknown variables (in the layers).

We adopt the same assumptions as in Buland and Omre (2003) and Grana et al. (2021). We assume that the error $\boldsymbol{\varepsilon}$ is distributed according to a Gaussian distribution $\boldsymbol{\varepsilon} \sim \mathcal{N}(\boldsymbol{\varepsilon}; \mathbf{0}, \boldsymbol{\Sigma}_\varepsilon)$ with $\mathbf{0}$ mean and covariance matrix $\boldsymbol{\Sigma}_\varepsilon$. We also assume that the prior distributions of the elastic attributes $\mathbf{f}$, $\mathbf{s}$, and $\boldsymbol{\rho}$ are log-Gaussian with temporal correlation. Hence, the concatenated vector $\mathbf{m} = [\ln \mathbf{f}, \ln \mathbf{s}, \ln \boldsymbol{\rho}]^T$, of length $n_m = 3(n_t + 1)$, is a multivariate Gaussian distribution $\mathbf{m} \sim \mathcal{N}(\mathbf{m}; \boldsymbol{\mu}_m, \boldsymbol{\Sigma}_m)$ with prior mean $\boldsymbol{\mu}_m$ and prior covariance matrix $\boldsymbol{\Sigma}_m$. The prior mean $\boldsymbol{\mu}_m = [\boldsymbol{\mu}_f, \boldsymbol{\mu}_s, \boldsymbol{\mu}_\rho]^T$ is a vector of length $n_m = 3(n_t + 1)$, where $\boldsymbol{\mu}_f$, $\boldsymbol{\mu}_s$, and $\boldsymbol{\mu}_\rho$ are the vectors of prior means of the logarithm of $\mathbf{f}$, $\mathbf{s}$, and $\boldsymbol{\rho}$, and represent the low-frequency models of the elastic attributes. The low-frequency (prior) models are computed from sonic and density logs by filtering velocity and density using Backus average (in time domain) and applying the transformations in equations 8 and 9. The prior covariance matrix $\boldsymbol{\Sigma}_m = \mathrm{cov}_{\mathbf{m}(t),\mathbf{m}(s)}$ includes the covariances of the logarithm of elastic properties and time covariances at times $t$ and $s$ based on a time-correlation model. For example, the prior covariance matrix $\boldsymbol{\Sigma}_m$ can be defined as $\boldsymbol{\Sigma}_m = \boldsymbol{\Sigma}_0 \otimes \boldsymbol{\Sigma}_t$ of the time-invariant covariance matrix of the logarithm of elastic attributes $\boldsymbol{\Sigma}_0$ and the time-dependent correlation matrix $\boldsymbol{\Sigma}_t$ defined by the time-correlation function $v(|t - s|)$ as in Buland and Omre (2003), where $\otimes$ is the Kronecker product. The matrix $\boldsymbol{\Sigma}_0$ has dimensions $(3 \times 3)$, whereas the matrix $\boldsymbol{\Sigma}_t$ has dimensions $(n_t + 1 \times n_t + 1)$; hence, the covariance matrix $\boldsymbol{\Sigma}_m$ has dimensions $(n_m \times n_m)$.

According to this assumption, the posterior distribution of the elastic attributes $\mathbf{m}$ conditioned on the seismic data $\mathbf{d}$ is a Gaussian

distribution $\mathbf{m}|\mathbf{d} \sim \mathcal{N}(\mathbf{m}; \boldsymbol{\mu}_{m|d}, \boldsymbol{\Sigma}_{m|d})$, and the posterior mean $\boldsymbol{\mu}_{m|d}$ and posterior covariance matrix $\boldsymbol{\Sigma}_{m|d}$ are given by

$$\boldsymbol{\mu}_{m|d} = \boldsymbol{\mu}_m + (\mathbf{W}\mathbf{A}\boldsymbol{\Sigma}'_m)^T \boldsymbol{\Sigma}_d^{-1}(\mathbf{d} - \boldsymbol{\mu}_d), \tag{13}$$

$$\boldsymbol{\Sigma}_{m|d} = \boldsymbol{\Sigma}_m - (\mathbf{W}\mathbf{A}\boldsymbol{\Sigma}'_m)^T \boldsymbol{\Sigma}_d^{-1} \mathbf{W}\mathbf{A}\boldsymbol{\Sigma}'_m, \tag{14}$$

where $\boldsymbol{\Sigma}'_m$ is the first derivative of the covariance matrix $\boldsymbol{\Sigma}_m$ (Buland and Omre, 2003; Grana et al., 2021). Using log-Gaussian transformations, the expression of the maximum a posteriori estimate $\hat{\mathbf{m}}$ of the elastic attributes becomes

$$\hat{\mathbf{m}} = \exp(\boldsymbol{\mu}_{m|d} - \boldsymbol{\sigma}^2_{m|d}). \tag{15}$$

By applying Bayesian linearized *f-s-r* inversion, we obtain the most likely values of the fluid factor $f$, the rigidity factor $s$, and the density $\rho$.

## Canonical correlation analysis

In practical applications, the physical relations between the elastic attributes (fluid factor $f$, rigidity factor $s$, and density $\rho$) and the petrophysical properties (porosity $\phi$, mineral volumes, and fluid saturations) are generally unknown and their approximations through rock-physics models are challenging. For this reason, we propose the application of CCA to infer the relationship between the measured variables $\mathbf{X}$ (i.e., the elastic attributes) and the unknown variables $\mathbf{Y}$ (i.e., the petrophysical properties) from the cross covariance of measurements and unknowns. In this work, we assume that the petrophysical properties of interest are porosity $\phi$, clay volume $v_c$, and water saturation $s_w$, but the approach can be extended to any finite set of variables.

Given two sets of variables $\mathbf{X} = [\mathbf{x}_1, \ldots, \mathbf{x}_n]$ and $\mathbf{Y} = [\mathbf{y}_1, \ldots, \mathbf{y}_m]$, for example, $\mathbf{X} = [\mathbf{f}, \mathbf{s}, \boldsymbol{\rho}]$ and $\mathbf{Y} = [\boldsymbol{\phi}, \mathbf{v}_c, \mathbf{s}_w]$, their cross covariance is given by $\boldsymbol{\Sigma}_{X,Y} = \mathrm{cov}(\mathbf{X}, \mathbf{Y})$, where each element $\sigma_{i,j} = \mathrm{cov}(\mathbf{x}_i, \mathbf{y}_j)$ for $i = 1, \ldots, n$ and $j = 1, \ldots, m$. CCA finds two vectors, $\hat{\mathbf{a}}$ of length $n$ and $\hat{\mathbf{b}}$ of length $m$, that maximize the correlation $c$ between $\mathbf{U} = \mathbf{X}\hat{\mathbf{a}}$ and $\mathbf{V} = \mathbf{Y}\hat{\mathbf{b}}$ as

$$(\hat{\mathbf{a}}, \hat{\mathbf{b}}) = \mathrm{argmax}_{\mathbf{a},\mathbf{b}}(c(\mathbf{X}\mathbf{a}, \mathbf{Y}\mathbf{b})). \tag{16}$$

The variables $\mathbf{U}$ and $\mathbf{V}$ are referred to as the first pair of canonical variables. CCA then finds two more vectors, uncorrelated with the first pair of canonical variables, that maximize the correlation in equation 16, to obtain the second pair of canonical variables. This process may be iterated $n_C = \min(n, m)$ times. The derivation is based on the Cauchy-Schwarz inequality and can be found in Thompson (1984). Its implementation is based on the singular value decomposition, and discussions can be found in statistical texts such as Jolliffe (2002) and Izenman (2008).

In the context of petrophysical inversion, we apply CCA to a training data set (e.g., a set of core samples or a subset of well-log data) containing the $n$ measured variables (e.g., $\mathbf{X}^{\mathrm{tr}} = [\mathbf{f}^{\mathrm{tr}}, \mathbf{s}^{\mathrm{tr}}, \boldsymbol{\rho}^{\mathrm{tr}}]$ with $n = 3$) and the $m$ unknown variables (e.g., $\mathbf{Y}^{\mathrm{tr}} = [\boldsymbol{\phi}^{\mathrm{tr}}, \mathbf{v}_c^{\mathrm{tr}}, \mathbf{s}_w^{\mathrm{tr}}]$ with $m = 3$) to determine the pairs of canonical variables $(\mathbf{U}_i^{\mathrm{tr}}, \mathbf{V}_i^{\mathrm{tr}})$ for $i = 1, \ldots, \min(n, m)$. For each pair of canonical variables $(\mathbf{U}_i^{\mathrm{tr}}, \mathbf{V}_i^{\mathrm{tr}})$, we compute a linear regression:

$$\begin{aligned}(\hat{\alpha}_i, \hat{\beta}_i) &= \mathrm{argmin}_{\alpha_i,\beta_i} \|\tilde{\mathbf{V}}_i^{\mathrm{tr}} - \mathbf{V}_i^{\mathrm{tr}}\| \\ &= \mathrm{argmin}_{\alpha_i,\beta_i} \|(\alpha_i \mathbf{U}_i^{\mathrm{tr}} + \beta_i) - \mathbf{V}_i^{\mathrm{tr}}\|.\end{aligned} \tag{17}$$

By definition of the CCA canonical variables, the regression coefficients $\hat{\alpha}_i$ should converge to one, whereas the regression coefficients $\hat{\beta}_i$ should converge to zero for $i = 1, \ldots, \min(n, m)$, although, in practical applications, they might not be exactly equal to these values due to numerical approximations. We then compute the canonical variables $\mathbf{U}_i$ of the seismic attributes obtained in the Bayesian linearized *f-s-r* inversion $\mathbf{X} = [\mathbf{f}, \mathbf{s}, \boldsymbol{\rho}]$, i.e., as $\mathbf{U}_i = \mathbf{X}\hat{\mathbf{a}}_i$ for $i = 1, \ldots, \min(n, m)$ and the corresponding canonical variables of the petrophysical parameters $\tilde{\mathbf{V}}_i = \hat{\alpha}_i \mathbf{U}_i + \hat{\beta}_i$. Finally, we compute the predictions of the petrophysical properties as $\mathbf{Y} = \tilde{\mathbf{V}}(\hat{\mathbf{b}})^{-1}$.

Figure 2 shows an example of application of CCA for the prediction of petrophysical properties from synthetic well-log data generated according to the stiff-sand model (Gal et al., 1998). The properties of interest are porosity, clay volume, and water saturation. We test the approach with two different data sets: the *f-s-r* parameterization in terms of the fluid and rigidity factors and density, and the Aki-Richards' parameterization in terms of P- and S-wave velocities and density. The training data set is extracted from well logs, and it includes 25% of the total number of well-log samples (randomly selected). Overall, the predictions obtained from fluid and rigidity factors and density are more accurate. The correlations between actual measurements and predictions are as follows: 0.99 for water saturation, 0.98 for clay volume, and 0.99 for porosity for the *f-s-r* parameterization, and 0.84 for water saturation, 0.90 for clay volume, and 0.95 for porosity for the Aki-Richards' parameterization.

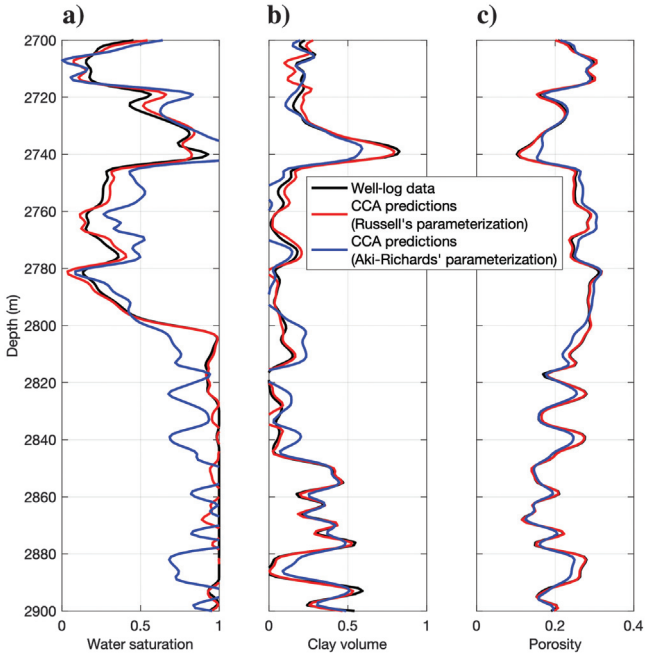


Figure 2. Petrophysical properties prediction from well-log data using CCA: (a) water saturation, (b) clay volume, and (c) porosity. The black lines represent the actual well logs, the red lines represent the CCA predictions from *f-s-r* elastic attributes (fluid and rigidity factors and density), and the blue lines represent the CCA predictions from Aki-Richards' elastic attributes (P- and S-wave velocities and density).

By applying CCA to the results of the Bayesian linearized *f-s-r* inversion, we obtain the predictions of the petrophysical properties, such as porosity $\phi$, clay volume $v_c$, and water saturation $s_w$. Because the transformations $\mathbf{U} = \mathbf{X}\hat{\mathbf{a}}$, $\tilde{\mathbf{V}}_i = \hat{\alpha}_i \mathbf{U}_i + \hat{\beta}_i$, and $\mathbf{Y} = \tilde{\mathbf{V}}(\hat{\mathbf{b}})^{-1}$ are linear, then the petrophysical properties $\mathbf{Y}$ can be written as a linear combination of the elastic properties $\mathbf{X}$:

$$\mathbf{Y} = \mathrm{K}\mathbf{X} + \Lambda, \tag{18}$$

and the proposed approach can be directly formulated in a Bayesian setting. Indeed, if $\mathbf{X}$ is a multivariate Gaussian distribution $\mathcal{N}(\mathbf{X}; \boldsymbol{\mu}_X, \boldsymbol{\Sigma}_X)$ with mean $\boldsymbol{\mu}_X$ and covariance matrix $\boldsymbol{\Sigma}_X$, then its linear transformation $\mathbf{Y}$ is a multivariate Gaussian distribution $\mathcal{N}(\mathbf{Y}|\mathbf{X}; \boldsymbol{\mu}_{Y|X}, \boldsymbol{\Sigma}_{Y|X})$ with conditional mean $\boldsymbol{\mu}_{Y|X}$ and conditional covariance matrix $\boldsymbol{\Sigma}_{Y|X}$ given by, respectively,

$$\boldsymbol{\mu}_{Y|X} = \mathrm{K}\boldsymbol{\mu}_X + \Lambda, \tag{19}$$

$$\boldsymbol{\Sigma}_{Y|X} = \mathrm{K}^T \boldsymbol{\Sigma}_X^{-1} \mathrm{K}. \tag{20}$$

We can then combine the results of the Bayesian linearized *f-s-r* inversion with the Bayesian approach to CCA to predict the posterior distribution of petrophysical properties from seismic data $P(\mathbf{r}|\mathbf{d})$. If we indicate with $\mathbf{r}$ the petrophysical properties, $\mathbf{m}$ the elastic properties, and $\mathbf{d}$ the seismic data, then the Bayesian linearized *f-s-r* inversion provides the posterior distribution $P(\mathbf{m}|\mathbf{d})$ of elastic properties given the seismic data, and the Bayesian approach to CCA provides the conditional distribution $P(\mathbf{r}|\mathbf{m})$ of petrophysical properties conditioned by elastic properties. According to our assumptions, $P(\mathbf{m}|\mathbf{d})$ is a multivariate log-Gaussian distribution and $P(\mathbf{r}|\mathbf{m})$ is a multivariate Gaussian distribution. Then, the posterior distribution of petrophysical properties $P(\mathbf{r}|\mathbf{d})$ given the seismic data is computed using the Chapman-Kolmogorov equation (Grana and Della Rossa, 2010):

$$P(\mathbf{r}|\mathbf{d}) = \int P(\mathbf{r}|\mathbf{m}) P(\mathbf{m}|\mathbf{d}) d\mathbf{m}, \tag{21}$$

where we assume that $P(\mathbf{m}|\mathbf{d}) = P(\mathbf{m}|\mathbf{d}, \mathbf{r})$ as the seismic data only depend on the seismic attributes. Equation 21 allows propagating the uncertainty from seismic data to petrophysical predictions through the seismic *f-s-r* model and the CCA-based implicit rock-physics model.

## APPLICATION

We test the method by applying the petrophysical inversion to a synthetic data set generated from a set of well-log data measured in a borehole in the Norwegian Sea. The well-log data set is shown in Figure 3. The interval under consideration includes an oil-saturated clastic reservoir and a shaley layer at the bottom of the reservoir. The main reservoir layer is located between approximately 1.82 and 1.86 s, and it shows relatively high porosity values with low clay volume and a small percentage of irreducible water saturation. It also includes an interbedded shaley layer in the upper part. The lower shaley interval shows lower porosity values with higher clay content and it is fully saturated with water. The elastic properties are computed according to the stiff-sand model (Gal et al., 1998; Dvorkin et al., 2014). The fluid factor is computed using equation 8, $f = (\rho V_\mathrm{P})^2 - \gamma_{\mathrm{dry}}^2 (\rho V_\mathrm{S})^2$, and the rigidity factor is computed using equation 9, $s = \gamma_{\mathrm{dry}}^2 (\rho V_\mathrm{S})^2$, where the parameter $\gamma_{\mathrm{dry}}^2$ is approximated using the stiff-sand model (Gal et al., 1998). Figure 4 shows the calculated fluid and rigidity factors as well as the synthetic partially stacked seismic data for three angle stacks corresponding to 10° (near stack), 23° (midstack), and 35° (far stack). The synthetic seismic data are generated as the convolution of a Ricker wavelet with dominant frequency of 45 Hz and the linearized approximation of Zoeppritz equations.

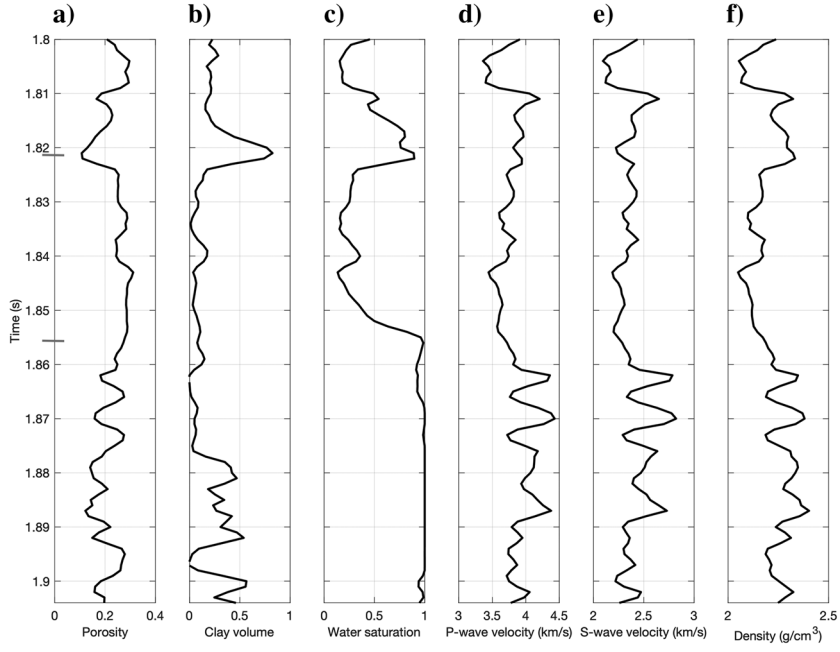


Figure 3. Well-log data in time domain: (a) porosity, (b) clay volume, (c) water saturation, (d) P-wave velocity, (e) S-wave velocity, and (f) density. The gray markers show the top and the bottom of the main reservoir.

We first apply the Bayesian linearized *f-s-r* inversion. The prior model for the mean of the elastic parameters is obtained by filtering the well-log curves of fluid and rigidity factors and density using Backus average to obtain the low-frequency trend of the model variables, whereas the prior covariance matrix is estimated from the actual well logs. The results of the inversion are shown in Figure 5 and show high accuracy in the predictions, especially in the main reservoir (from 1.82 to 1.86 s). In the lower part of the interval, the abrupt transitions of porosity and clay volume in the interbedded layers below seismic resolution are not accurately captured, but the overall trend is correctly detected. Figure 5 also shows the 0.90 confidence interval of the Bayesian linearized inversion. The inversion is relatively precise for the rigidity factor and density with coverage ratios slightly greater than 0.9, whereas for the fluid factor the uncertainty is slightly overestimated with coverage ratio close

to 1, possibly due to the variability of the pore volume in the bottom part of the interval. We then apply CCA to predict the petrophysical properties of interest. The pairs of canonical variables are calculated based on the petrophysical well-log data in Figure 3 and the elastic attributes in Figure 4. The training data set includes 25% of the well-log samples (randomly selected). Because we apply CCA to two sets of three variables, we obtain three pairs of canonical variables (Figure 6). Their correlations are 0.9998, 0.9952, and 0.9692. The results of the petrophysical inversion for porosity, clay volume, and water saturation are shown in Figure 7. Despite the limitations due to the limited bandwidth of seismic data, the inversion results are accurate for water saturation and porosity, especially in the upper part, whereas clay volume is not fully resolved, possibly due to the low correlation between the rigidity factor and the clay volume (Figure 2). The correlations between the actual measurements and the predictions are as follows: 0.83 for porosity, 0.64 for clay volume, and 0.97 for water saturation. Figure 7 also shows the 0.90 confidence interval of the CCA-based Bayesian inversion. The posterior variance is slightly overestimated for water saturation and porosity with coverage ratio close to 1. The elastic properties predicted from the inversion results are shown in Figure 8 and compared with the actual well logs and the upscaled well logs and show a satisfactory match at the seismic resolution.

To assess the accuracy of the inversion, we compare the results to two different inversion methods: a Bayesian linearized AVO inversion with CCA and a Bayesian linearized AVO inversion with a rock-physics model. First, we apply a Bayesian linearized AVO inversion based on Aki-Richards' linearized approximation to obtain the maximum a posteriori estimates of P- and S-wave velocities and density, as proposed in Buland and Omre (2003). The results of the seismic inversion are shown in Figure 9 and show an accurate prediction of the elastic properties, consistent with the band-limited nature of seismic data. The uncertainty is slightly underestimated with coverage ratio less than 0.90. Then, we apply CCA between the set of elastic properties, i.e., P- and S-wave velocities and density, and the set of petrophysical properties of interest, i.e., porosity, clay volume, and water saturation. The inversion results are shown in Figure 10. The inversion captures the overall trend of the petrophysical properties, but the predictions are less accurate than the proposed method based on the *f-s-r* parameterization. Indeed, the correlations between actual measurements and predictions are as follows: 0.71 for porosity, 0.45 for clay volume, and 0.93 for water saturation. Compared with the results in Figure 7 obtained with the proposed method based on the *f-s-r* parameterization, the posterior uncertainty of the petrophysical properties is overall narrower and underestimated, especially for water saturation, possibly due to the regression of the predictions toward the mean. In the second comparison, we calibrate a rock-physics model and apply a Bayesian rock-physics inversion (Grana et al., 2021) based on a truncated Gaussian prior distribution and using the same rock-physics model, i.e., the stiff-sand model (Gal et al., 1998; Dvorkin et al., 2014), used to generate the synthetic data. The results of the Bayesian rock-physics inversion are shown in Figure 11. The inversion performs relatively well in the bottom part of the data set and predicts

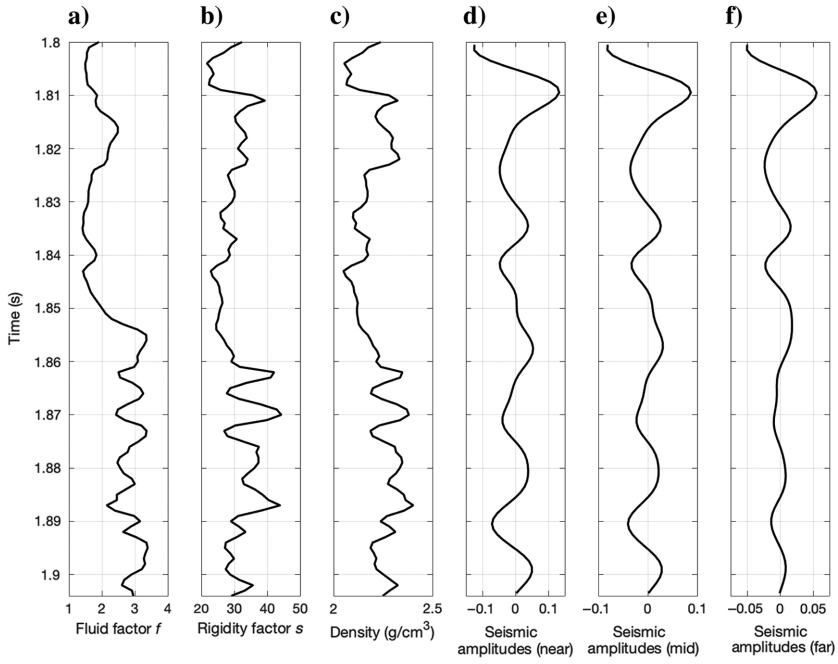


Figure 4. Elastic attributes in time domain and synthetic seismic data: (a) fluid factor, (b) rigidity factor, (c) density, (d) near seismic amplitudes, (e) midseismic amplitudes, and (f) far seismic amplitudes.

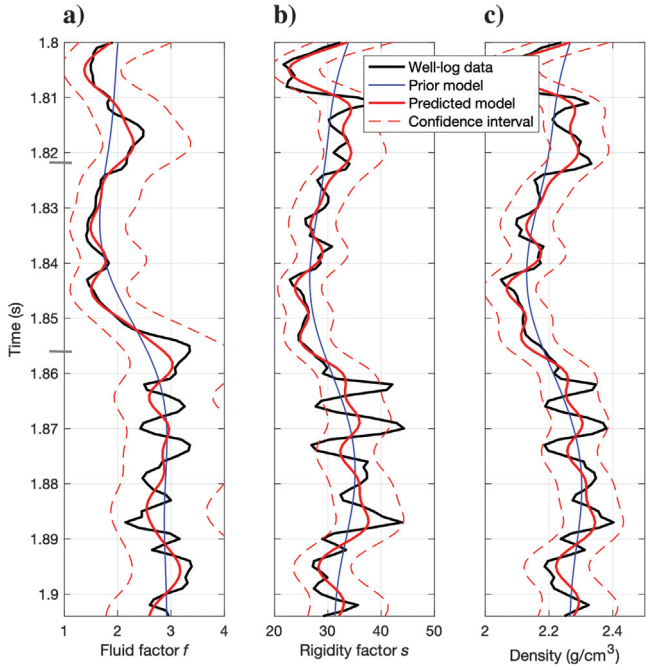


Figure 5. Bayesian linearized *f-s-r* inversion: (a) fluid factor, (b) rigidity factor, and (c) density. The black lines represent the actual well logs, the red lines represent the maximum a posteriori model from the Bayesian linearized inversion, and the blue lines represent the prior model. The dashed lines represent the 0.90 confidence interval. The gray markers show the top and the bottom of the main reservoir.

the petrophysical variations in the interbedded layer; however, the results are less accurate overall than the proposed method, especially for water saturation. The water saturation predictions show a larger local variability and a regression toward the mean value, similar to the results obtained in Figure 10. The correlations between the actual measurements and the predictions are as follows: 0.85 for porosity, 0.86 for clay volume, and 0.73 for water saturation. Due to the nonlinearity of the rock-physics model, the analytical expression of the 0.90 confidence interval is not available for the Bayesian rock-physics inversion.

As in Buland and Omre (2003) and Grana and Della Rossa (2010), the proposed inversion can be extended according to a trace-by-trace approach, leading to an efficient inversion algorithm for 2D and 3D seismic data sets. We demonstrate the applicability of the method to a 2D partially stacked seismic line acquired in an oil-saturated clastic reservoir in the Norwegian Sea. The data set includes three angle stacks, corresponding to average angles of 10° (near stack), 23° (midstack), and 35° (far stack) and it is shown in Figure 12. The three wavelets are extracted from each angle stack independently, and they are zero phase with dominant frequencies equal to 24, 22, and 21 Hz. The sampling rate of the seismic data is

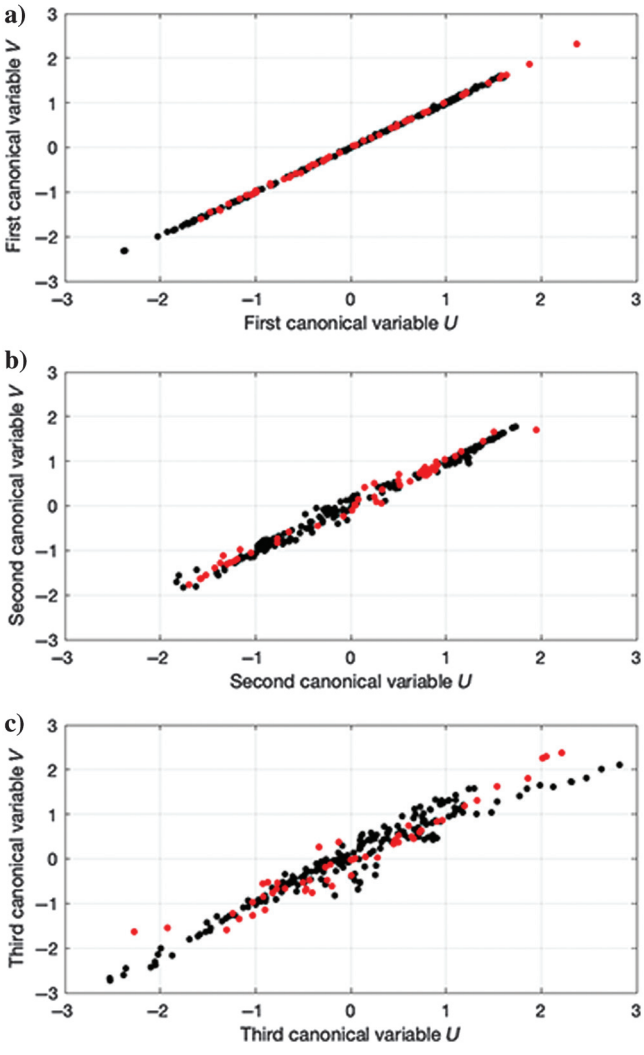


Figure 6. Pairs of canonical variables obtained by applying CCA to *f-s-r* elastic attributes and petrophysical properties. The red dots represent the training data set (25% of the well logs), and the black dots represent the full well-log data set.

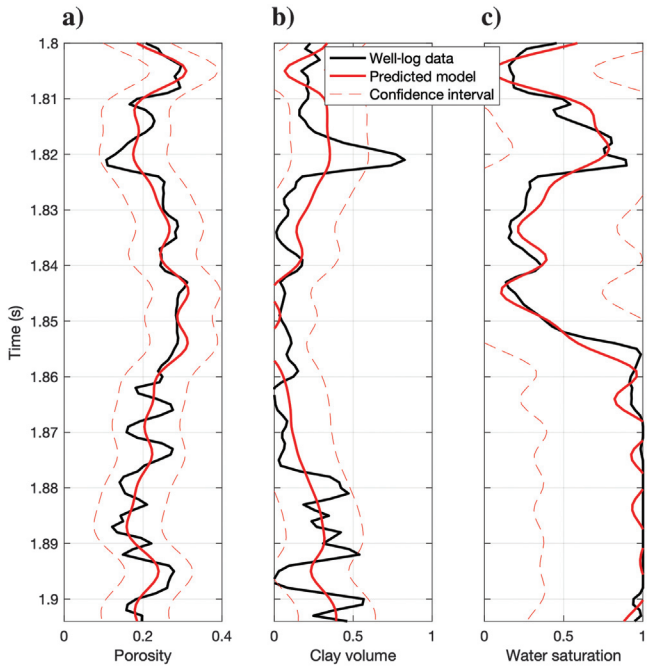


Figure 7. CCA predictions from *f-s-r* elastic attributes: (a) porosity, (b) clay volume, and (c) water saturation. The black lines represent the actual well logs and the red lines represent the predictions from CCA. The dashed lines represent the 0.90 confidence interval.

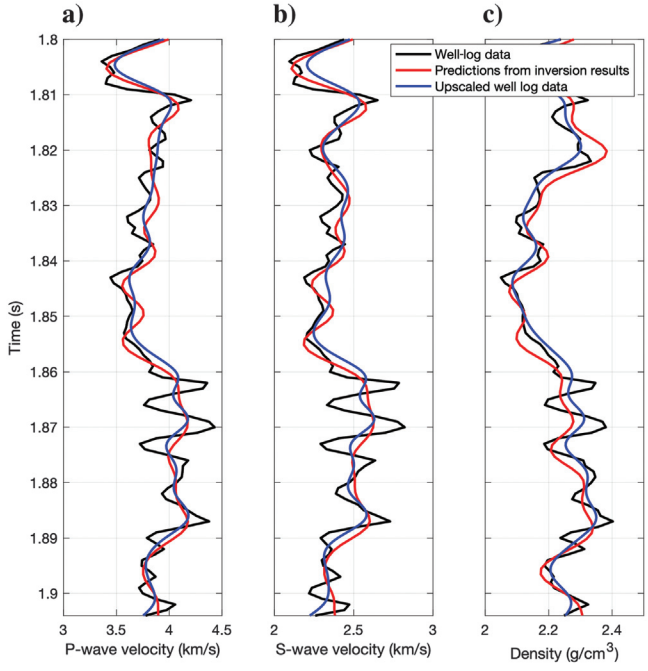


Figure 8. Elastic properties predictions from CCA-based inversion results: (a) P-wave velocity, (b) S-wave velocity, and (c) density. The black lines represent the actual well logs, the red lines represent the predictions from the inverted results in Figure 7, and the blue lines represent the upscaled well logs.

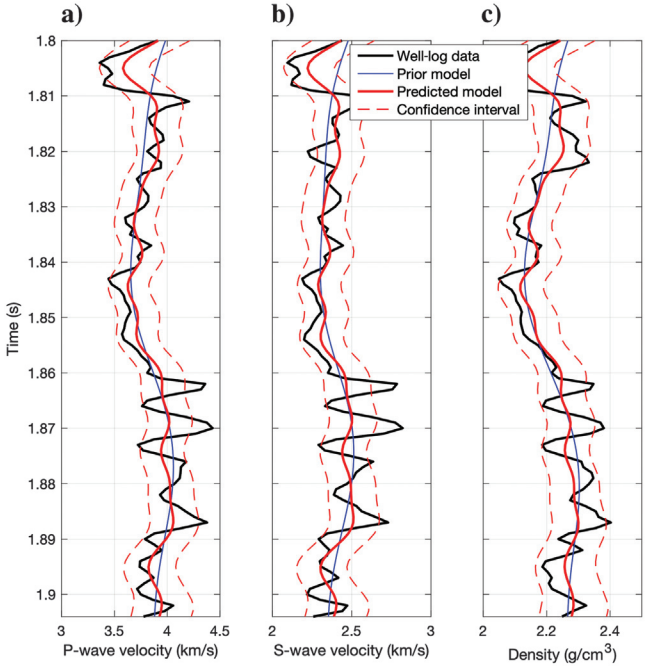


Figure 9. Bayesian linearized AVO inversion: (a) P-wave velocity, (b) S-wave velocity, and (c) density. The black lines represent the actual well logs, the red lines represent the maximum a posteriori model from the Bayesian linearized inversion, and the blue lines represent the prior model. The dashed lines represent the 0.90 confidence interval.

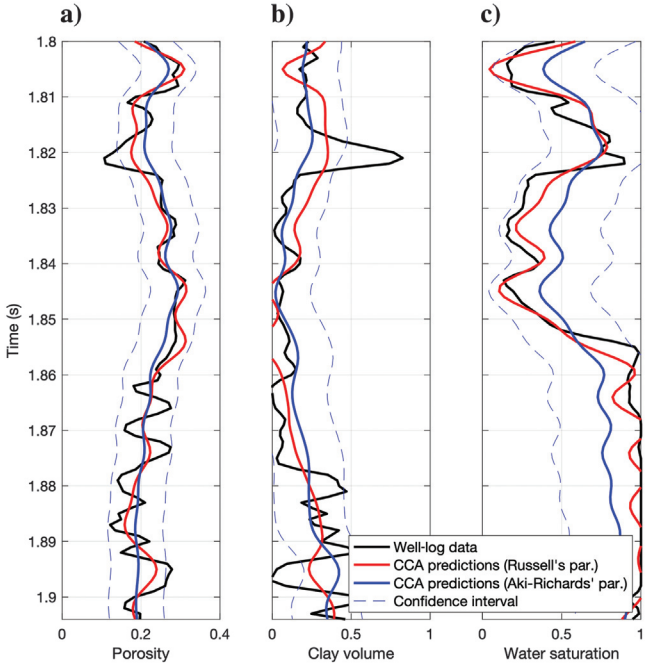


Figure 10. CCA predictions from Aki-Richards' elastic attributes: (a) porosity, (b) clay volume, and (c) water saturation. The black lines represent the actual well logs, and the red lines represent the predictions from CCA. The blue lines represent the results in Figure 7 and are shown for comparison. The dashed lines represent the 0.90 confidence interval.

4 ms, and the signal-to-noise ratio is approximately 2. The low-frequency model of the elastic properties is obtained by filtering the well-log data with a maximum frequency of 10 Hz and interpolating the filtered data along the seismically interpreted horizon, whereas the prior distribution of the petrophysical properties is estimated from the well-log data. The inversion results for porosity, clay volume, and water saturation are shown in Figure 13 and compared with the upscaled well-log data. Overall, the inversion results match the upscaled well-log data for water saturation and porosity, whereas clay volume is slightly underestimated in the interbedded shaley layers.

## DISCUSSION

The proposed methodology combines two useful tools: the Bayesian *f-s-r* seismic inversion and the Bayesian CCA-based petrophysical inversion. The main advantage of the Bayesian *f-s-r* seismic data compared with the Bayesian linearized AVO inversion based on the traditional Aki-Richards approximation (Buland and Omre, 2003) is the high correlation between the predicted elastic parameters and the reservoir petrophysical properties, in particular between the fluid factor and the water saturation. The fluid factor is an effective tool for discriminating fluids, especially in gas-saturated reservoirs (Russell et al., 2011), but it also can be used in other applications with different fluid conditions. The ability of the fluid factor to discriminate between fluids in the reservoir depends on several factors, including the spatial distribution of the fluid components in the mixture and the variability of the pore volume. In a homogeneous mixture of gas and water, the fluid factor can

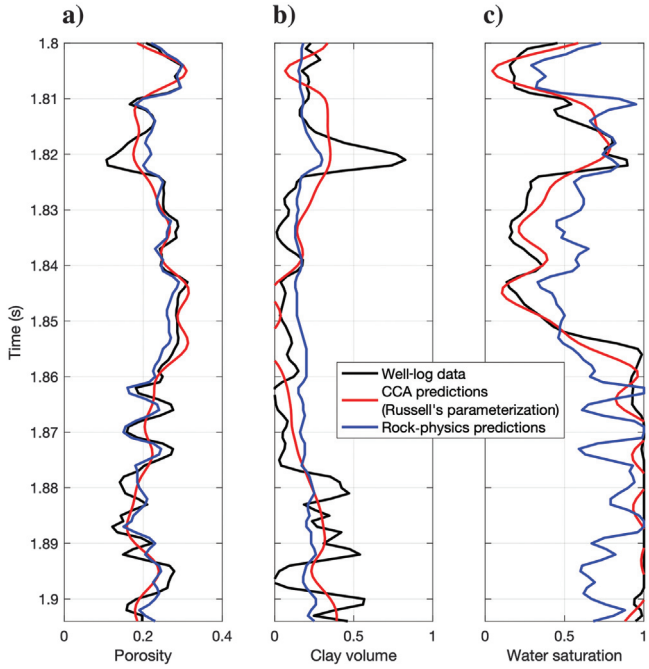


Figure 11. Rock-physics inversion predictions from Aki-Richards' elastic attributes: (a) porosity, (b) clay volume, and (c) water saturation. The black lines represent the actual well logs, and the red lines represent the predictions from CCA. The blue lines represent the results in Figure 7 and are shown for comparison.

discriminate fully water-saturated rock from fully gas-saturated rocks, but it might fail to discriminate partially saturated rocks from fully gas-saturated rocks, whereas, in patchy mixtures, the fluid factor can discriminate the fluid saturations, as the fluid factor response is approximately linear with respect to the fluid modulus, hence water saturation. The CCA-based petrophysical inversion and its Bayesian formulation are a powerful tool for the prediction of the petrophysical properties in the absence of an explicit rock physics. CCA is an efficient method to find a transformation of the measured properties and variables of interest in a domain where the transformed variables are highly linearly correlated. As the transformation is linear, the inversion is extremely efficient, and the Bayesian formulation can be naturally extended to the CCA-based petrophysical inversion. Because the result of the Bayesian seismic inversion is a log-Gaussian distribution and the result of the Bayesian petrophysical inversion is a Gaussian distribution, to combine the two probability distributions and propagate the uncertainty from the seismic domain to the petrophysical domain, it is necessary to numerically compute the posterior probability using the integral of the product of the two distributions (equation 21); however, this integral can be efficiently computed in a discretized domain using matrix multiplications, as shown in Grana et al. (2021). Overall, we recommend testing multiple elastic parameterizations for the application of CCA to identify the set of elastic parameters with the highest correlation in the CCA transformed domain. The Bayesian linearized AVO approximation can then be extended to the chosen parameterization, by modifying the forward seismic operator, and the Bayesian CCA-based petrophysical inversion can be applied to the seismic inversion results.

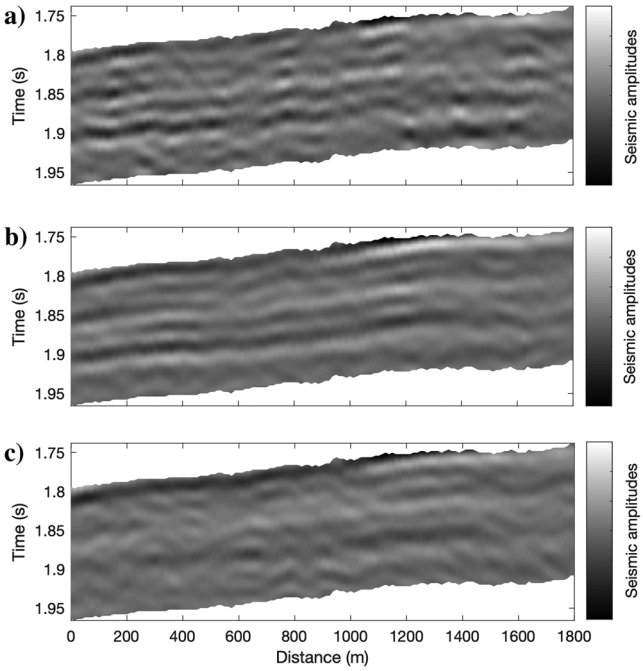


Figure 12. Partially stacked seismic data measured in an oil-saturated clastic reservoir in the Norwegian Sea: (a) near seismic amplitudes (10°), (b) midseismic amplitudes (23°), and (c) far seismic amplitudes (35°).

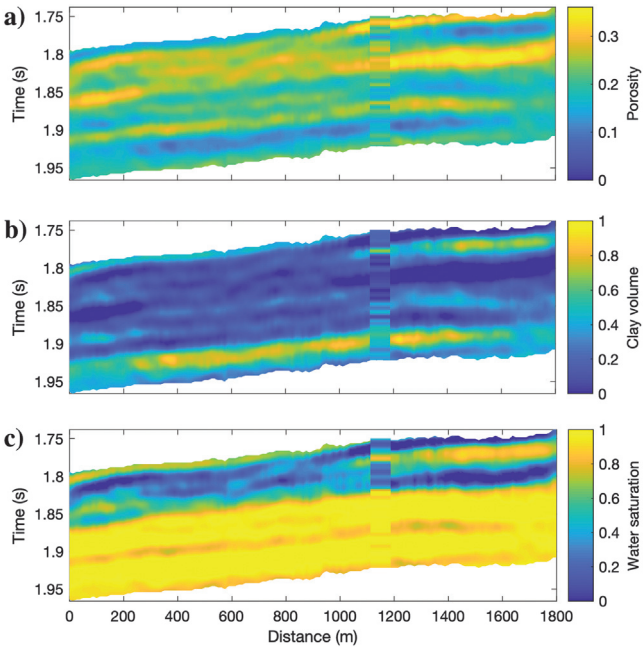


Figure 13. Petrophysical inversion results along the 2D seismic line in Figure 12: (a) porosity, (b) clay volume, and (c) water saturation. The superimposed column represents the upscaled well-log data.

## CONCLUSION

We have presented an innovative inversion combining a Bayesian linearized AVO approach for seismic inversion and CCA for the prediction of petrophysical properties from partially stacked seismic data. The proposed approach is built on the Bayesian linearized AVO inversion and the *f-s-r* linearized AVO approximation. By combining these two methods, we can predict a set of elastic attributes that are correlated with the petrophysical properties of interest. The novelty of the proposed approach is the application of CCA to the parameterization of the seismic inversion in terms of fluid and rigidity factors, which provides an implicit rock-physics model for the seismic reservoir characterization of petrophysical properties. CCA is used to find canonical variates (linear combinations of original variables) that maximize the correlation between the predictor variables (elastic attributes) and the response variables (petrophysical properties). Indeed, as CCA is derived directly from the well-log data, this approach does not require the calibration of an explicit rock-physics model. Furthermore, the CCA-based petrophysical inversion is applied in a Bayesian framework, which can be integrated with the Bayesian *f-s-r* linearized AVO inversion to propagate the uncertainty from seismic data to petrophysical properties. The proposed method allows predicting petrophysical properties with higher accuracy compared with traditional methods. The *f-s-r* AVO linearization includes a fluid factor term that is highly correlated with the water saturation, which can improve the seismic reservoir characterization in terms of the fluid distribution. The proposed approach can be extended to any combination of elastic attributes and any petrophysical parameterization, as CCA finds linear transformations of the input properties that maximize their correlation.

## ACKNOWLEDGMENTS

Dario Grana acknowledges the School of Energy Resources of the University of Wyoming, the Nielson Energy Fellowship and BP, sponsor of the Bayesian Learning Consortium. Tapan Mukerji acknowledges the sponsors of the Stanford Center for Earth Resources Forecasting (SCERF) and support from Steve Graham, the Dean of the Stanford School of Earth, Energy and Environmental Sciences. Brian Russell acknowledges the support of GeoSoftware.

## DATA AND MATERIALS AVAILABILITY

Data associated with this research are available and can be obtained by contacting the corresponding author.

## APPENDIX A

## DISCRETE CONVOLUTIONAL MODEL

In the discrete convolution in equations 10 and 11, the matrix $\mathbf{A}$ is a sparse block matrix of dimensions $(n_\theta n_t \times 3n_t)$:

$$\mathbf{A} = \begin{bmatrix} \mathbf{A}_f(\theta_1) & \mathbf{A}_s(\theta_1) & \mathbf{A}_r(\theta_1) \\ \vdots & \vdots & \vdots \\ \mathbf{A}_f(\theta_{n_\theta}) & \mathbf{A}_s(\theta_{n_\theta}) & \mathbf{A}_r(\theta_{n_\theta}) \end{bmatrix}, \tag{A-1}$$

where $\mathbf{A}_f(\theta_i)$, $\mathbf{A}_s(\theta_i)$, and $\mathbf{A}_r(\theta_i)$ are diagonal matrices of dimensions $(n_t \times n_t)$:

$$\mathbf{A}_f(\theta_i) = \begin{bmatrix} c_f(\theta_i) & \dots & 0 \\ \vdots & \ddots & \vdots \\ 0 & \dots & c_f(\theta_i) \end{bmatrix},$$
$$\mathbf{A}_s(\theta_i) = \begin{bmatrix} c_s(\theta_i) & \dots & 0 \\ \vdots & \ddots & \vdots \\ 0 & \dots & c_s(\theta_i) \end{bmatrix}, \tag{A-2}$$
$$\mathbf{A}_r(\theta_i) = \begin{bmatrix} c_r(\theta_i) & \dots & 0 \\ \vdots & \ddots & \vdots \\ 0 & \dots & c_r(\theta_i) \end{bmatrix},$$

with diagonal elements equal to $c_f(\theta_i)$, $c_s(\theta_i)$, and $c_r(\theta_i)$, given in equation 7, for $i = 1, \dots, n_\theta$.

The first-order differential matrix $\mathbf{D}$ is a sparse block matrix of dimensions $(3n_t \times n_m)$:

$$\mathbf{D} = \begin{bmatrix} \mathbf{D}_b & 0 & 0 \\ 0 & \mathbf{D}_b & 0 \\ 0 & 0 & \mathbf{D}_b \end{bmatrix}, \tag{A-3}$$

with three blocks $\mathbf{D}_b$ of size $(n_t \times n_t + 1)$ on the main diagonal:

$$\mathbf{D}_b = \begin{bmatrix} -1 & 1 & 0 & \dots & 0 \\ 0 & -1 & 1 & \ddots & \vdots \\ \vdots & \ddots & \ddots & \ddots & 0 \\ 0 & \dots & 0 & -1 & 1 \end{bmatrix}. \tag{A-4}$$

The wavelet matrix $\mathbf{W}$ is a sparse band matrix of dimensions $(n_\theta n_t \times n_\theta n_t)$:

$$\mathbf{W} = \begin{bmatrix} \mathbf{W}_1(\theta_1) & \dots & 0 \\ \vdots & \ddots & \vdots \\ 0 & \dots & \mathbf{W}_{n_\theta}(\theta_{n_\theta}) \end{bmatrix}, \tag{A-5}$$

where the block $\mathbf{W}_i$ of size $(n_t \times n_t)$ contains the wavelet for the angle $\theta_i$:

$$\mathbf{W}_i(\theta_i) = \begin{bmatrix} w_i(t_1) & \dots & 0 & \dots & 0 \\ \vdots & \ddots & \vdots & \vdots & \vdots \\ \vdots & \vdots & w_i(t_1) & \vdots & \vdots \\ \vdots & \vdots & \vdots & \ddots & \vdots \\ w_i(t_{n_w}) & \vdots & \vdots & \vdots & w_i(t_1) \\ \vdots & \ddots & \vdots & \vdots & \vdots \\ \vdots & \vdots & w_i(t_{n_w}) & \vdots & \vdots \\ \vdots & \vdots & \vdots & \ddots & \vdots \\ 0 & \dots & 0 & \dots & w_i(t_{n_w}) \end{bmatrix}, \tag{A-6}$$

for $i = 1, \dots, n_\theta$, as shown in Buland and Omre (2003) and Grana et al. (2021).

## REFERENCES

Aki, K., and P. G. Richards, 2002, Quantitative seismology, 2nd ed.: W. H. Freeman and Co.

Aleardi, M., and F. Ciabarri, 2017, Assessment of different approaches to rock-physics modeling: A case study from offshore Nile Delta: Geophysics, **82**, no. 1, MR15–MR25, doi: 10.1190/geo2016-0194.1.

Aleardi, M., F. Ciabarri, and R. Calabrò, 2018a, Two-stage and single-stage seismic-petrophysical inversions applied in the Nile Delta: The Leading Edge, **37**, 510–518, doi: 10.1190/tle37070510.1.

Aleardi, M., F. Ciabarri, and T. Gukov, 2018b, A two-step inversion approach for seismic-reservoir characterization and a comparison with a single-loop Markov-chain Monte Carlo algorithm: Geophysics, **83**, no. 3, R227–R244, doi: 10.1190/geo2017-0387.1.

Alvarez, P., F. Bolívar, F. M. Di Luca, and T. Salinas, 2015, Multiattribute rotation scheme: A tool for reservoir property prediction from seismic inversion attributes: Interpretation, **3**, no. 4, SAE9–SAE18, doi: 10.1190/INT-2015-0029.1.

Avseth, P., T. Mukerji, and G. Mavko, 2010, Quantitative seismic interpretation: Applying rock physics tools to reduce interpretation risk: Cambridge University Press.

Bachrach, R., 2006, Joint estimation of porosity and saturation using stochastic rock-physics modeling: Geophysics, **71**, no. 5, O53–O63, doi: 10.1190/1.2235991.

Biot, M. A., 1941, General theory of three-dimensional consolidation: Journal of Applied Physics, **12**, 155–164, doi: 10.1063/1.1712886.

Bornard, R., F. Allo, T. Coléou, Y. Freudenreich, D. H. Caldwell, and J. G. Hamman, 2005, Petrophysical seismic inversion to determine more accurate and precise reservoir properties: Presented at the Europec/EAGE Annual Conference, SPE, SPE 94144.

Bortfeld, R., 1961, Approximations to the reflection and transmission coefficients of plane longitudinal and transverse waves: Geophysical Prospecting, **9**, 485–502, doi: 10.1111/j.1365-2478.1961.tb01670.x.

Bosch, M., 1999, Lithologic tomography: From plural geophysical data to lithology estimation: Journal of Geophysical Research, **104**, 749–766, doi: 10.1029/1998JB900014.

Bosch, M., C. Carvajal, J. Rodrigues, A. Torres, M. Aldana, and J. Sierra, 2009, Petrophysical seismic inversion conditioned to well-log data: Methods and application to a gas reservoir: Geophysics, **74**, no. 2, O1–O15, doi: 10.1190/1.3043796.

Buland, A., and H. Omre, 2003, Bayesian linearized AVO inversion: Geophysics, **68**, 185–198, doi: 10.1190/1.1543206.
Buland, A., O. Kolbjørnsen, R. Hauge, Ø. Skjæveland, and K. Duffaut, 2008, Bayesian lithology and fluid prediction from seismic prestack data: Geophysics, **73**, no. 3, C13–C21.
Coléou, T., F. Allo, R. Bornard, J. Hamman, and D. Caldwell, 2005, Petrophysical seismic inversion: 75th Annual International Meeting, SEG, Expanded Abstracts, 1355–1358, doi: 10.1190/1.2147938.
Connolly, P. A., 1999, Elastic impedance: The Leading Edge, **18**, 438–452, doi: 10.1190/1.1438307.
Connolly, P. A., and M. J. Hughes, 2016, Stochastic inversion by matching to large numbers of pseudo-wells: Geophysics, **81**, no. 2, M7–M22, doi: 10.1190/geo2015-0348.1.
Dvorkin, J., M. A. Gutierrez, and D. Grana, 2014, Seismic reflections of rock properties: Cambridge University Press.
Fatti, J. L., P. J. Vail, G. C. Smith, P. J. Strauss, and P. R. Levitt, 1994, Detection of gas in sandstone reservoirs using AVO analysis: A 3-D seismic case history using the glowstick technique: Geophysics, **59**, 1362–1376, doi: 10.1190/1.1443695.
Fjeldstad, T., and D. Grana, 2018, Joint probabilistic petrophysics-seismic inversion based on Gaussian mixture and Markov chain prior models: Geophysics, **83**, no. 1, R31–R42, doi: 10.1190/geo2017-0239.1.
Fournier, F., and J. F. Derain, 1995, A statistical methodology for deriving reservoir properties from seismic data: Geophysics, **60**, 1437–1450, doi: 10.1190/1.1443878.
Gal, D., J. Dvorkin, and A. Nur, 1998, A physical model for porosity reduction in sandstones: Geophysics, **63**, 454–459, doi: 10.1190/1.1444346.
Gassmann, F., 1951, Uber die elastizitat poroser medien: Vierteljahrsschrift der Naturforschenden Gesellschaft in Zurich, **96**, 1–23.
Gidlow, P. M., G. C. Smith, and P. J. Vail, 1992, Hydrocarbon detection using fluid factor traces: A case history: How useful is AVO analysis? EAGE Summer Research Workshop on How Useful is Amplitude-Versus-Offset (AVO) Analysis, 78–89.
González, E. F., T. Mukerji, and G. Mavko, 2008, Seismic inversion combining rock physics and multiple-point geostatistics: Geophysics, **73**, no. 1, R11–R21, doi: 10.1190/1.2803748.
Goodway, W. N., T. Chen, and J. Downton, 1997, Improved AVO fluid detection and lithology discrimination using Lamé petrophysical parameters ; "λρ", "μρ", & "λ/μ fluid stack", from P and S inversions: 67th Annual International Meeting, SEG, Expanded Abstracts, 183–186, doi: 10.1190/1.1885795.
Grana, D., 2016, Bayesian linearized rock-physics inversion: Geophysics, **81**, no. 6, D625–D641, doi: 10.1190/geo2016-0161.1.
Grana, D., and E. Della Rossa, 2010, Probabilistic petrophysical-properties estimation integrating statistical rock physics with seismic inversion: Geophysics, **75**, no. 3, O21–O37, doi: 10.1190/1.3386676.
Grana, D., T. Fjeldstad, and H. Omre, 2017, Bayesian Gaussian mixture linear inversion for geophysical inverse problems: Mathematical Geosciences, **49**, 493–515, doi: 10.1007/s11004-016-9671-9.
Grana, D., T. Mukerji, and P. Doyen, 2021, Seismic reservoir modeling: Wiley.
Gray, F., T. Chen, and W. Goodway, 1999, Bridging the gap: Using AVO to detect changes in fundamental elastic constants: 69th Annual International Meeting, SEG, Expanded Abstracts, 852–855, doi: 10.1190/1.1821163.
Gunning, J., and M. Glinsky, 2007, Detection of reservoir quality using Bayesian seismic inversion: Geophysics, **72**, no. 3, R37–R49, doi: 10.1190/1.2713043.
Hampson, D. P., B. H. Russell, and B. Bankhead, 2005, Simultaneous inversion of pre-stack seismic data: 75th Annual International Meeting, SEG, Expanded Abstracts, 1633–1636, doi: 10.1190/1.2148008.
Hardoon, D. R., S. Szedmak, and J. Shawe-Taylor, 2004, Canonical correlation analysis: An overview with application to learning methods: Neural Computation, **16**, 2639–2664, doi: 10.1162/0899766042321814.
Izenman, A. J., 2008, Modern multivariate statistical techniques: Regression, classification and manifold learning: Springer Science + Business Media LLC.
Jolliffe, I. T., 2002, Principal component analysis, 2nd ed.: Springer-Verlag.
Knott, C. G., 1899, Reflection and refraction of elastic waves, with seismological applications: Philosophical Magazine, London, **48**, 567–569.
Krief, M., J. Garat, J. Stellingwerff, and J. Ventre, 1990, A petrophysical interpretation using the velocities of P and S waves (full-waveform sonic): The Log Analyst, **31**, 355–369.
Mavko, G., T. Mukerji, and J. Dvorkin, 2020, The rock physics handbook: Tools for seismic analysis in porous media, 2nd ed.: Cambridge University Press.
Mazzotti, A., and E. Zamboni, 2003, Petrophysical inversion of AVA data: Geophysical Prospecting, **51**, 517–530, doi: 10.1046/j.1365-2478.2003.00389.x.
Mukerji, T., A. Jørstad, P. Avseth, G. Mavko, and J. R. Granli, 2001, Mapping lithofacies and pore-fluid probabilities in a North Sea reservoir: Seismic inversions and statistical rock physics: Geophysics, **66**, 988–1001, doi: 10.1190/1.1487078.
Purkait, B., and D. D. Majumdar, 2014, Distinguishing different sedimentary facies in a deltaic system: Sedimentary Geology, **308**, 53–62, doi: 10.1016/j.sedgeo.2014.05.001.
Richards, P. G., and C. W. Frasier, 1976, Scattering of elastic waves from depth-dependent inhomogeneities: Geophysics, **41**, 441–458, doi: 10.1190/1.1440625.
Rimstad, K., P. Avseth, and H. Omre, 2012, Hierarchical Bayesian lithology/fluid prediction: A North Sea case study: Geophysics, **77**, no. 2, B69–B85, doi: 10.1190/geo2011-0202.1.
Russell, B., 1988, Introduction to seismic inversion methods: SEG.
Russell, B., K. Hedlin, F. Hilterman, and L. Lines, 2003, Fluid-property discrimination with AVO: A Biot-Gassmann perspective: Geophysics, **68**, 29–39, doi: 10.1190/1.1543192.
Russell, B. H., D. Gray, and D. P. Hampson, 2011, Linearized AVO and poroelasticity: Geophysics, **76**, no. 3, C19–C29, doi: 10.1190/1.3555082.
Satija, A., C. Scheidt, L. Li, and J. Caers, 2017, Direct forecasting of reservoir performance using production data without history matching: Computational Geosciences, **21**, 315–333, doi: 10.1007/s10596-017-9614-7.
Shuey, R. T., 1985, A simplification of the Zoeppritz equations: Geophysics, **50**, 609–614, doi: 10.1190/1.1441936.
Spikes, K., T. Mukerji, J. Dvorkin, and G. Mavko, 2008, Probabilistic seismic inversion based on rock physics models: Geophysics, **72**, no. 5, R87–R97, doi: 10.1190/1.2760162.
Stolt, R. H., and A. B. Weglein, 1985, Migration and inversion of seismic data: Geophysics, **50**, no. 12, 2458–2472.
Thompson, B., 1984, Canonical correlation analysis: Uses and interpretation: Sage.
Whitcombe, D. N., P. A. Connolly, R. L. Reagan, and T. C. Redshaw, 2002, Extended elastic impedance for fluid and lithology prediction: Geophysics, **67**, 63–67, doi: 10.1190/1.1451337.
Wu, J., T. Mukerji, and A. Journel, 2005, Prediction of spatial patterns of saturation time-lapse from time-lapse seismic, *in* O. Leuangthong and C. V. Deutsch, eds., Geostatistics Banff 2004: Springer Publication, 671–680.
Yin, Z., S. Strebelle, and J. Caers, 2020, Automated Monte Carlo-based quantification and updating of geological uncertainty with borehole data (AutoBEL v1.0): Geoscientific Model Development, **13**, 651–672, doi: 10.5194/gmd-13-651-2020.
Zoeppritz, K., 1919, Erdbebenwellen VIII B, Uber die reflexion und durchgang seismischer welling durch Unstetigkeitsflachen: Gottinger Nachr, **1**, 66–84.

Biographies and photographs of the authors are not available.